JACS
JOURNAL OF THE AMERICAN CHEMICAL SOCIETY
Article
pubs.acs.org/JACS

Direct Observation of Short-Range Structural Coherence During a Charge Transfer Induced Spin Transition in a CoFe Prussian Blue Analogue by Transmission Electron Microscopy

Miho Itoi,*[,†] Toyoharu Jike,[†] Daisuke Nishio-Hamane,[‡] Seiichi Udagawa,[†] Tetsuya Tsuda,[§] Susumu Kuwabata,[§] Kamel Boukheddaden,[∥] Matthew J. Andrus,[⊥] and Daniel R. Talham*[,⊥]

[†]Division of Physics, Institute of Liberal Education, Nihon University School of Medicine, Tokyo 173-8610, Japan

[‡]Institute for Solid State Physics, The University of Tokyo, Chiba 277-8581, Japan

[§]Department of Applied Chemistry, Graduate School of Engineering, Osaka University, Suita, Osaka 565-0871, Japan

[∥]Groupe d'Etudes de la Matière Condensée, UMR 8635, CNRS-Université de Versailles Saint-Quentin-en-Yvelines, 45 Avenue des Etats Unis, 78035 Versailles, France

[⊥]Department of Chemistry, University of Florida, P.O. Box 117200, Gainesville, Florida 32611-7200, United States

Supporting Information

ABSTRACT: The local structure within the Co−Fe atomic array of the photoswitchable coordination polymer magnet, $K_{0.3}Co[Fe(CN)_6]_{0.77}\cdot nH_2O$, is directly observed during charge transfer induced spin transition (CTIST), a solid−solid phase change, using high-resolution transmission electron microscopy (HRTEM). Along with the low-spin (LS) or thermally quenched high-spin (HS) states normally observed in CTIST solids at low temperature, slow cooling of $K_{0.3}Co[Fe(CN)_6]_{0.77}\cdot nH_2O$ results in an intermediate phase containing both HS and LS domains with short coherence length. By mapping individual metal−metal distances, the nanometer-scale HS domains are directly visualized within the LS array. Temperature-dependent analyses allow monitoring of HS domain coarsening along the warming branch of the CTIST, providing direct visualization of the elastic process and insight into the mechanism of phase propagation. Normally sensitive to electron beam damage, the low-temperature TEM measurements of the porous coordination polymer are enabled by using appropriate ionic liquids instead of usual conductive thin-film coatings, an approach that should find general utility in related classes of materials.

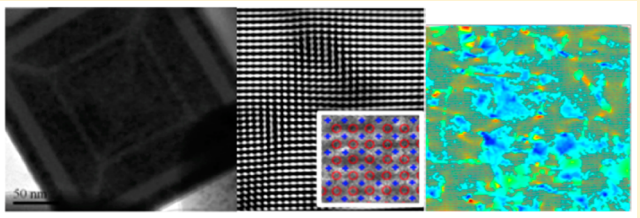

INTRODUCTION

Direct observation of local atomic structure is expected to give deep insights into how short-range interactions and mesoscale cooperative effects relate to macroscopic responses in materials. Metal−organic coordination polymer materials present a special case as their elastic lattice structure is strongly coupled to their functional properties such as sorption, ion storage, catalysis, magnetism, and external-field switchable magnetism.[1] In parallel, functional coordination polymer or metal−organic framework heterostructures such as nanocomposites, core−shell particles, or thin films have been developed in recent years for which interfacial structural characteristics influence physical properties.[2] Atomic-level investigations will be critical for full understanding of how macroscopic behavior relates to local structure, local lattice dynamics, and phonon propagation in these mesoscale materials. The present study uses high-resolution transmission electron microscopy (TEM) to directly monitor the distribution of interatomic distances during a structural phase transition in a coordination polymer solid, gaining insight into the elastic distribution of the different phases. The study is enabled by coating the coordination polymer particles with an ionic liquid (IL) in the TEM, stabilizing the porous solids against normally observed degradation under high-vacuum conditions.

Prussian blue analogues (PBAs) are prototypical porous coordination polymer solids, which have attracted considerable recent attention in studies of alkali ion storage,[3] negative thermal expansion, and photoswitchable molecular magnetism.[4,5] The family of cobalt hexacyanoferrates (CoFe−PBAs), Scheme 1, is well-known for light-switchable magnetism, whereby a charge transfer induced spin transition (CTIST) between the $Fe^{III}LS-CN-Co^{II}HS$ (referred to here as the high-spin or HS state) and $Fe^{II}LS-CN-Co^{III}LS$ (low-spin or LS state) states alters magnetization. The CTIST is also associated with a large structural transformation resulting from the change in Co−N bond distance in the two spin states.[6,7] The states can be interconverted thermally, between the high-temperature HS state and low-temperature LS state, or optically from the LS state to a metastable HS state below a

Received: August 5, 2015
Published: October 28, 2015

DOI: 10.1021/jacs.5b08242
J. Am. Chem. Soc. 2015, 137, 14686−14693

Scheme 1. Parent CoFe–PBA Structure, $KCo[Fe(CN)_6]$[a]

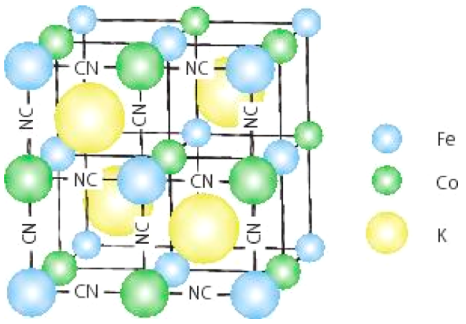

[a]The Co–NC–Fe frame makes a 3D cubic structure with counterions in the tetrahedral sites. In the case of the title compound, $K_{0.3}Co[Fe(CN)_6]_{0.77}\cdot nH_2O$, 0.23 of the $[Fe(CN)_6]$ octahedral sites are vacant and replaced by coordinating water molecules and the occupancy of the K atoms (Wyckoff site 8 of the *Fm*3*m* space group) is 0.3.

characteristic relaxation temperature. The high-spin CoFe–PBAs magnetically order at low temperature, so they represent still rare examples of light-switchable magnets.[6]

The CTIST in the CoFe–PBAs is strongly coupled to the lattice, so details of the transition depend on composition, including the choice of counterion and extent of cyanometallate vacancies. For the present study, we have chosen to investigate the unusual behavior of the nonstoichiometric analogue $K_{0.3}Co[Fe(CN)_6]_{0.77}\cdot nH_2O$, which has been shown to exhibit *multistability* with three interconvertible states at low temperatures: a quenched high-spin state (Q) reached by rapid cooling, a low-spin state (LT) accessed by the thermal decay of the Q state, and an intermediate state (IM) achieved by slow cooling from room temperature (Figure 1).[8] The Q and IM states magnetically order (Figure S1 and Table S1).[8b] In the IM state, HS and LS fractions coexist due to an elastic stress associated with the large volume change of the CTIST.[9] It has been shown that particle size influences the appearance of the IM state, although the relationship between HS and LS fractions within the lattice is still unclear.[10] Quantitative information on the elastic stress in the crystal during the IM state self-organization process will help to understand its appearance, as well as the conditions for stabilizing the Q state or LT state.

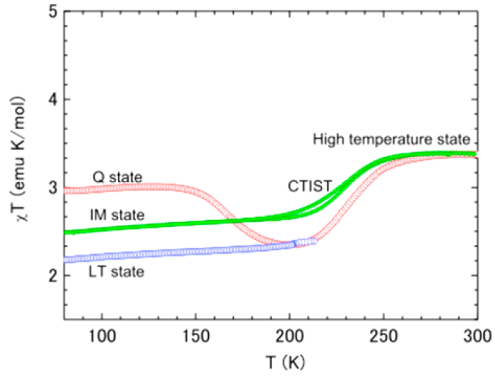

Figure 1. Temperature-dependent magnetic susceptibility of $K_{0.3}Co[Fe(CN)_6]_{0.77}\cdot nH_2O$ between 80 and 300 K. The mean particle size in the sample is approximately 135 nm. The quenched (Q) state, which has the $Co^{II}(S = 3/2)$–$Fe^{III}(S = 1/2)$, or HS, state is obtained by rapid cooling from room temperature to 10 K. The low-temperature $Co^{III}(S = 0)$–$Fe^{II}(S = 0)$, or LS, state is achieved from thermal control of the Q state. The IM state is obtained by slow cooling (1 K/min) from room temperature. The data and assignments are consistent with previous reports (refs 8a and 10).

The TEM described here is shown to give directly spatial information on the local microstructures at the atomic level. Although normally sensitive to the conditions of the TEM experiment, use of an appropriate ionic liquid is shown to lead to stable atomic-level TEM observations of the iron and cobalt atomic array during the CTIST for $K_{0.3}Co[Fe(CN)_6]_{0.77}\cdot nH_2O$ mesoscale particles. Direct observation of HS domain coarsening during the thermal LS → HS transition gives insight into the short structural coherence caused by the CTIST in the IM state and the elastic structure of the sample.

EXPERIMENTAL SECTION

The $K_{0.3}Co[Fe(CN)_6]_{0.77}\cdot nH_2O$ particles with average size of 135 nm (Figure S2) were prepared as described in previous papers.[8a,10] Transmission electron microscopy was performed with JEM-2100 and JEM-2010F microscopes (JEOL), using a voltage of 200 kV at the Institute for Solid State Physics of The University of Tokyo. Images were recorded with an imaging plate detector and CCD camera. The ionic liquids, for example $[(CH_3)_3NC_2H_4OH][CH_3C(OH)CO_2]$ (choline lactate, [Ch][Lac]), were diluted with water to 1 vol % of IL/water with ultrasonic agitation. The ionic liquid was micropipetted onto the $K_{0.3}Co[Fe(CN)_6]_{0.77}\cdot nH_2O$ particles on copper-conductive mesh grids (Nisshin EM). The grids were placed in an oven at 60 °C for ∼15 min to remove water from the IL droplet. Low-temperature TEM observations used a liquid He cooled specimen holder (JEOL). Stable TEM measurement could be carried out in the temperature range from ∼210 to 300 K. TEM image analysis was performed with free software ImageJ[11] for fast Fourier transformations and with an original imaging program written for Matlab for atomic position calculations.

RESULTS AND DISCUSSION

Ionic Liquids for TEM Analysis of CoFe–PBA Particles.

Transmission electron microscopy is used to observe microscopic and/or geometric structures for elastic strain evaluation in semiconductor device and nanoparticles.[12] However, electron irradiation causes heating, electrostatic charging, or ionization damage often making the measurement difficult.[13] Metal–organic coordination polymer solids like the CoFe–PBAs are especially susceptible to electron beam damage, even at very short exposure times. We have succeeded in achieving stable temperature-dependent TEM observations in $K_{0.3}Co[Fe(CN)_6]_{0.77}\cdot nH_2O$ by wetting the particles with an ionic liquid. The IL prevents the sample from melting or bursting when interacting with the electron beam. Also, compared to typical carbon or PtPb thin-film coatings, sample charging is reduced, leading to sharper and clearer TEM images.

Ionic liquids (Scheme 2) are widely studied and have found significant use in materials synthesis and analysis.[14] Since ILs have negligible vapor pressure, they can be used for analysis under vacuum conditions. Furthermore, as ILs are ionic conductors, they can protect samples from charging and heating during scanning electron microscopy (SEM) and TEM measurements. They have found use in SEM or TEM observations of biological samples that can be fragile under high vacuum or heavily distorted if dried.[15] ILs have also been recently applied for in situ TEM analysis of the growth mechanism of gold nanoparticles.[16] However, as far as we are aware, this is the first time ILs have been used to stabilize coordination polymer solids for electron microscopy.

DOI: 10.1021/jacs.5b08242
J. Am. Chem. Soc. 2015, 137, 14686–14693

Scheme 2. Cations and Anions of the Ionic Liquids Used in This Study

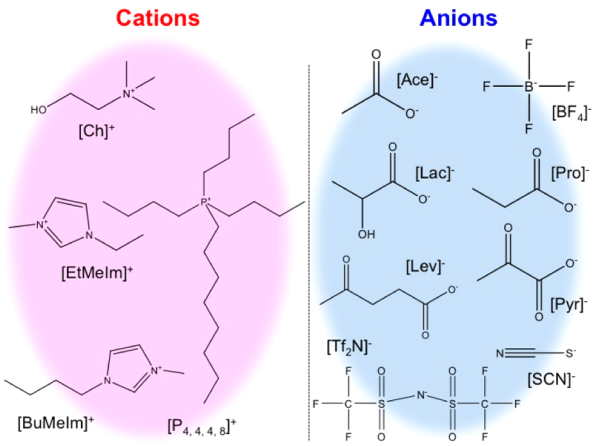

Several IL systems were explored to find suitable conditions for imaging the CoFe–PBA, including seven types of hydrophilic ionic liquids, two types of hydrophobic ionic liquids, as well as combinations with different additives (Table I). The identity and dilution ratio of the IL proved to be important parameters for clear TEM observation. Choline lactate and choline pyruvate were found to be effective ILs for the KCoFe–PBA particles that were studied. It is likely that the nature of surface absorption plays a role in the effectiveness of the IL. The range of conditions that were explored and those found to be most effective are described in Table I.

Particle Imaging and Local Spin-State Analysis. *1. TEM Images at Room Temperature.* The KCoFe–PBA structure has been well-investigated by powder X-ray diffraction (PXRD), neutron diffraction, and extended X-ray absorption fine structure (EXAFS)[7,8c,9] and shown to be a three-dimensional Fe–CN–Co cubic framework with a = 10.3 Å at room temperature.[9] Parts a–c of Figure 2 display TEM images of a $K_{0.3}Co[Fe(CN)_6]_{0.77}\cdot nH_2O$ particle under different magnifications at room temperature. Fringes associated with the cubic structure are clearly observed by using the ionic liquid [Ch][Lac]. Figure 2d is a 1500K magnification HRTEM image taken at 286 K, and a coherent shepherd-check pattern related to the alternating cobalt ion and iron ion atomic array is observed. There are also many random blurred regions in the crystal, probably caused by defects associated with $[Fe(CN)_6]^{3-/4-}$ octahedral vacancies. To extract atomic positions, the background of the TEM image is subtracted by first performing a fast Fourier transformation (FFT), Figure 2e, followed by inverse fast Fourier transformation (IFFT), Figure 2f, to give a weighted image of the lattice structure. Many defects randomly distributed on the crystal plane and an inhomogeneous strain distribution are observed. We calculated the atomic coordinates of the Co and/or Fe atoms under translation symmetry by using the points with brightest intensities, which are on centers of the Co–Fe square lattice in the bright-field images. The Co–Fe distances within the subcubic lattice structures are about ~5 Å, consistent with the Co–NC–Fe distance of 5.15 Å determined by X-ray diffraction.[9]

2. Temperature-Dependent TEM Measurements. To visualize HS domain nucleation and coarsening during the phase change, temperature-dependent TEM measurements were performed on the CTIST heating branch using a liquid He cooled specimen holder. The sample was gradually cooled to about 100 K to achieve the IM state (Figure 1) and then slowly heated to observe changes as the IM state transitions back to the room-temperature HS phase. The sample is easily damaged by the TEM experiment below the freezing point of the ionic liquid (~210 K), so the study is restricted to temperatures above this point (Figure 3).

Figure 4 shows 3D charts of Co–Fe distances on an ~900 nm^2 crystal plane along with histograms of the distribution of Co–Fe distances obtained at several temperatures. Note that the data have not been adjusted for TEM calibration, so measured values have a constant offset of 0.4–0.5 Å relative to the crystallographically determined distances. The color bar gradient spans the distances expected for the LS and HS states, and the transition from blue toward red relates to the LS → HS conversion. It should be noted that, according to magnetic susceptibility data, Figure 3, the low-temperature IM state initially contains about 33% HS sites, and upon warming to 235 K about 20% of the CTIST-active sites have transitioned. The 3D distribution map of Co–Fe distances confirms that the majority is still in the LS state at 235 K, and HS structures with short coherence are randomly distributed in the LS lattice.

The mean (uncorrected) Co–Fe lengths can be obtained from Gaussian fits to the histograms in Figure 4, parts e and f. At 235 K the mean distance is 4.439 Å with standard deviation (SD) of 0.067 Å. The mean bond length shifts to 4.535 Å (SD of 0.058 Å) at 250 K. After applying a constant calibration offset, the mean values are consistent with X-ray diffraction data, which showed ~5.06 Å at 235 K and 5.13 Å at 250 K for a sample of 500 nm particles.[9] According to the magnetic susceptibility measurement the CTIST is complete by 286 K, while the TEM image analysis shows the mean Co–Fe length of 4.602 Å (SD of 0.092 Å) still approaching the room-temperature value of 4.721 Å (SD of 0.046 Å). The discrepancy is likely a consequence of comparing a single particle to a bulk measurement representing an ensemble of particles.

The imaging of domains gives insight into the mechanism of the elastic phase transition and provides an opportunity to compare its progress to different models for cooperative spin transitions. In systems dominated by short-range interactions, transitions are barrier crossing processes requiring a nucleation event, and the key parameters determining the critical size of a nucleus are the interplay between its surface and bulk free energies. The nucleation of the new phase is more favorable at the surface (or around the defects) of the material than in the bulk. The density of nucleation sites is then expected to be larger at particle edges, although as a system becomes larger, nucleation in the bulk may dominate. On the other hand, when the spin-state changes are accompanied by adjustments in unit cell volume (bond lengths or molecular size), the local volume changes are delocalized over the lattice, causing long-range interactions.[17,18] For example, a recent model predicts an attractive interaction between two HS atom defects in a LS lattice of as much as 30 meV.[18]

The growth of HS domains in $K_{0.3}Co[Fe(CN)_6]_{0.77}\cdot nH_2O$ as it is warmed through the CTIST are clearly seen within the bulk of the particles in the TEM images (Figure 4). Sites were defined as in the HS state by a Co–Fe distance longer than 4.5 Å (L > 4.5 Å), since 99.9% of Co–Fe pairs satisfy this condition at 300 K. The spatial distribution of HS sites is visualized at four temperatures in Figure 4, and over larger regions at 235 and 250 K in Figure 5 for which the total calculated crystal plane size is about 2100 pixels (65.6 nm × 65.6 nm). In Figure

DOI: 10.1021/jacs.5b08242
J. Am. Chem. Soc. 2015, 137, 14686–14693

Table I. Analysis of the Efficiency of Different Ionic Liquids for TEM Measurements of KCoFe−PBA at Room Temperature

category	name	definitive dilution ratio	observation stability at 300 K (efficiency)[a]
hydrophilic ionic liquid	**1** choline lactate $[(CH_3)_3NC_2H_2OH][CH_3C(OH)CO_2]$, [Ch][Lac]	1:100 (with H_2O)	◎
	2	1:50 (with H_2O)	◎
	3 plus 10 vol % H_2O + choline dihydrogen phosphate	1:10 (with H_2O)	Δ
	4 plus 50 vol % H_2O + samarium sulfate	1:10 (with H_2O)	×
	5 plus 50 vol % H_2O + sodium chloride	1:10 (with H_2O)	○
	6 plus 50 vol % H_2O + choline dihydrogen phosphate	1:10 (with H_2O)	×
	7 plus 10 vol % H_2O + Pt nanoparticle	1:10 (with H_2O)	Δ
	8 choline propionate, [Ch][Pro]	1:100 (with H_2O)	Δ
	9	1:20 (with H_2O)	○
	10 choline levulinate, [Ch][Lev]	1:100 (with H_2O)	×
	11	1:20 (with H_2O)	Δ
	12 choline pyruvate, [Ch][Pyr]	1:100 (with H_2O)	Δ
	13	1:20 (with H_2O)	◎
	14 1-butyl-3-methylimizolium tetrafluoroborate, [BuMeIm][BF_4]	1:5 (with H_2O)	Δ
	15	1:10 (with H_2O)	×
	16 1-ethyl-3-methylimizolium acetate, [EtMeIm][Ace]	1:100 (with H_2O)	○
	17	1:20 (with H_2O)	○
	18 1-ethyl-3-methylimizolium lactate, [EtMeIm][Lac]	1:100 (with H_2O)	Δ
	19	1:20 (with H_2O)	Δ
hydrophobic ionic liquid	**20** tributyloctylphosphonium thiocyanate [P4,4,48][SCN]	undiluted solution	Δ
	21 tributyloctylphosphonium bis(trifluoromethanesulfonyl) amide [P4,4,48][Tf_2N]	undiluted solution	○
without IL	**22** carbon vapor deposition		Δ

[a]The effectiveness is qualitatively evaluated using four levels of stability under 120 kV/100K magnification continuous observation: ×, sample damaged within 1 min or unstable/poor image visibility; Δ, stable for 2 min; ○, stable for ∼3 min with clear image visibility; ◎, stable more than 4 min and clear image visibility.

J. Am. Chem. Soc. 2015, 137, 14686−14693
DOI: 10.1021/jacs.5b08242

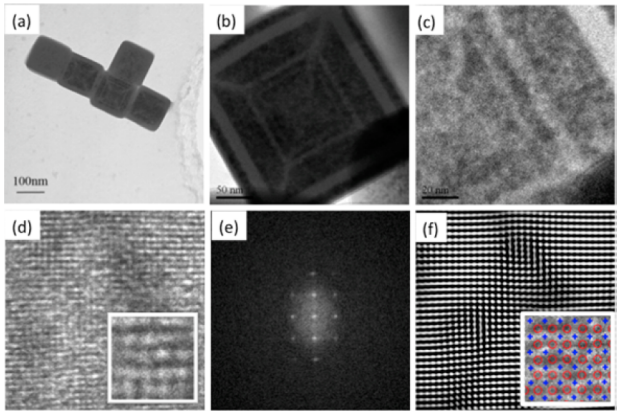

Figure 2. TEM images of $K_{0.3}Co[Fe(CN)_6]_{0.77}\cdot nH_2O$ using the ionic liquid $[(CH_3)_3NC_2H_4OH][CH_3C(OH)CO_2]$ ([Ch][Lac], 1 vol %). (a) The average particle size of $K_{0.3}Co[Fe(CN)_6]_{0.77}\cdot nH_2O$ is about ~135 nm. (b and c) Larger particles of $K_{0.3}Co[Fe(CN)_6]_{0.77}\cdot nH_2O$ at two magnifications at room temperature. (d) An HRTEM image at 286 K with 1500K magnification. A coherent checked pattern related to the alternating Co−Fe array is observed. (e) The reciprocal image of frame d obtained by Fourier transformation. (f) The periodic structure is extracted by Fourier filtering from panel e. Inset: a partial image of d with the Co and Fe atomic positions, dark spots in the TEM, indicated with red circles and the centers of Co−Fe cubic lattices, the empty suboctants corresponding to the Wyckoff site 8 of the *Fm*3*m* space group, indicated by the blue crosses.

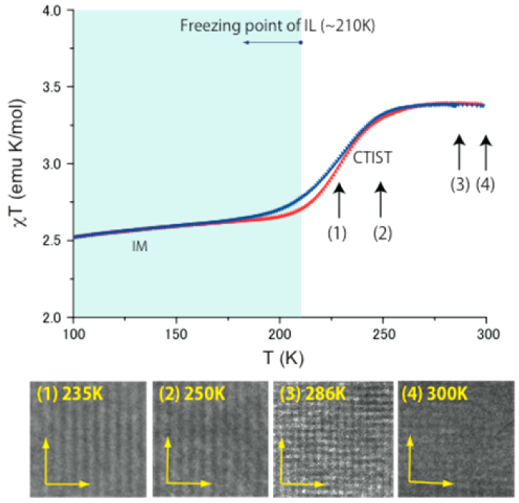

Figure 3. Temperature dependence of the magnetic susceptibility for $K_{0.3}Co[Fe(CN)_6]_{0.77}\cdot nH_2O$, measured while cooling (blue) to generate the IM phase or warming (red) at 1 K/min. The charge transfer induced spin transition is observed from ~180 to ~275 K on heating. Temperature-dependent TEM measurements were performed using ionic liquids during the heating branch from 220 to 300 K. $K_{0.3}Co[Fe(CN)_6]_{0.77}\cdot nH_2O$ is quite sensitive to the electron beam, so TEM observations could not be carried out below ~220 K (light blue region), the freezing point of the ionic liquid.

5, parts a and b, atoms corresponding to the $L > 4.5$ Å criterion are denoted with red marks on the color map. The average size of coherent HS structure at 235 K from Figure 5c is 534.5 Å^2, containing about 26 Co/Fe atoms, with the average Co−Fe distance of 4.572 Å. When increasing temperature, we observe the growth and coalescence of the HS domains. As a result, at 250 K, the number of small coherent HS structures decreased significantly while the average number of HS sites per domain

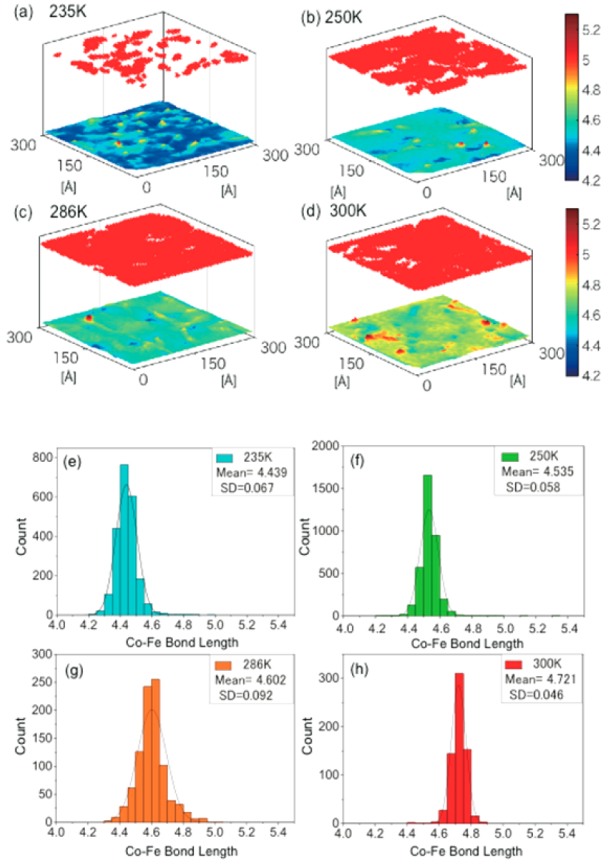

Figure 4. (a−d) 3D charts of the Co−Fe distances within approximately 30 nm × 30 nm crystal planes at several temperatures. The Co−Fe length at each site is measured as the average value between each atom site and its nearest neighbor atoms. The color scale represents the change from LS to HS. Above each map is a 2D array of red points marking the positions of HS atoms, chosen as those having Co−Fe distances longer than 4.5 Å. The number of HS atoms clearly increases with increasing temperature. Plots e−h are the corresponding histograms of Co−Fe lengths obtained from the 3D charts at several temperatures. Note that the distances are not corrected for TEM calibration and images correspond to different nanoparticles in the same sample batch.

increased up to ~373 atoms, with the average size reaching 7744 Å^2 (Figure 5d). On the basis of the 2D images in Figure 5, the HS fractions in the plane are estimated as 13% at 235 K, 76% at 250 K. Although quantitatively slightly different, these values parallel those from magnetic data, which result from the bulk response of the system.

A statistical analysis of the number of atoms in the each HS domain at 235 and 250 K is presented in Figure 5, parts c and d. The distribution is asymmetric, following a log-normal law at 235 K, characteristic of disordered systems[19] with aging properties. It can also be seen that the developing HS structures have short coherence length and do not show any clear spatial self-organization. Furthermore, the short coherence length structures are irregularly shaped. The 235 K images indicate that the IM phase is structurally disordered with residual HS domains embedded in a largely LS lattice. The present ramified structure contrasts with recent optical microscopy imaging on spin-crossover solids, and theoretical studies that show phases propagating from a nucleation point as a single domain.[20,21] From the viewpoint of the elastic process, these small HS domains inside the LS lattice can be considered

DOI: 10.1021/jacs.5b08242
J. Am. Chem. Soc. 2015, 137, 14686−14693

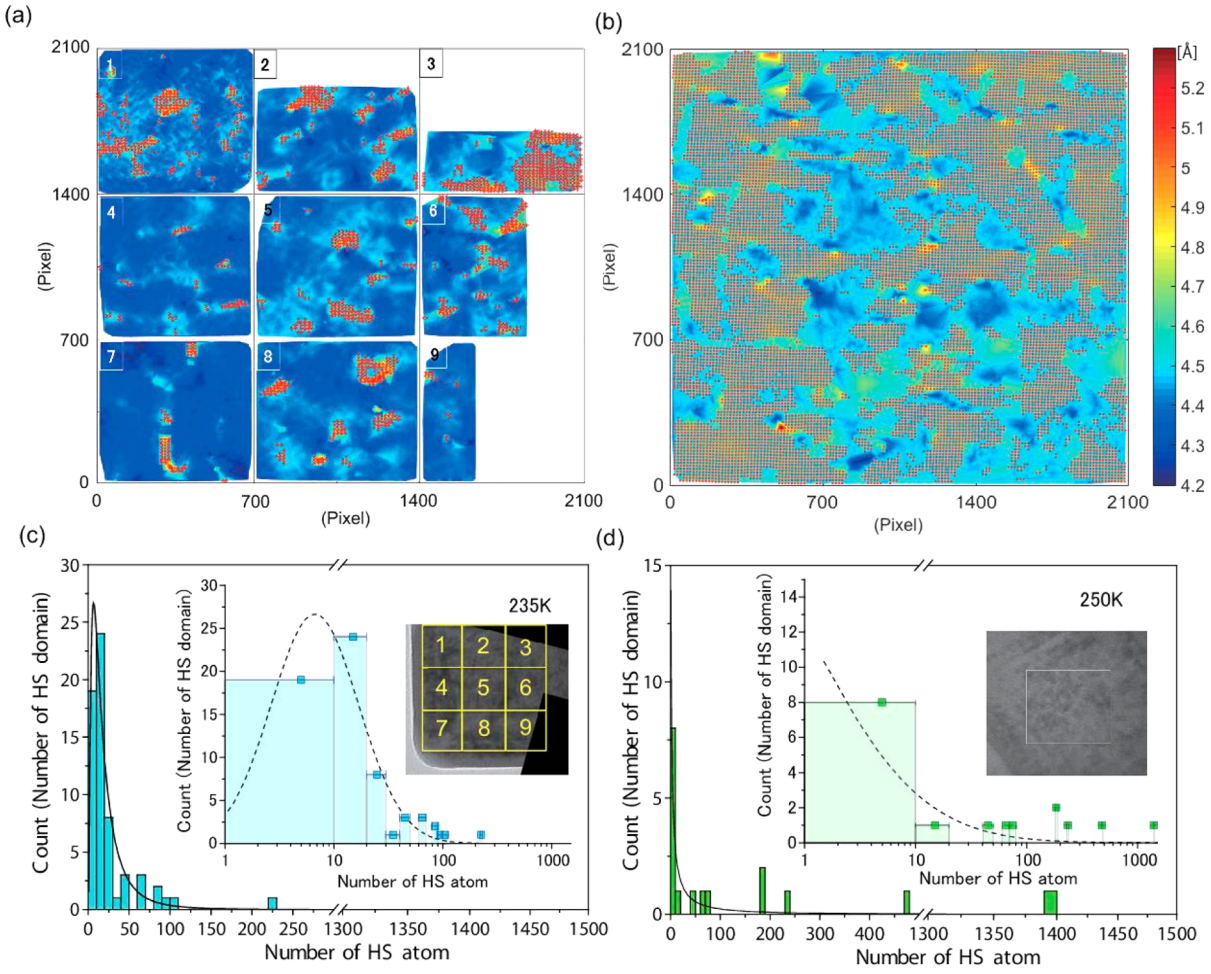

Figure 5. TEM image analysis of an ~2100 pixel × 2100 pixel (about 65.6 nm × 65.6 nm) crystal plane at (a) 235 K and (b) 250 K. The images correspond to different nanoparticles in the same sample batch. The color bar represents the average Co−Fe distance at each site. Co−Fe distances associated with HS atoms (L > 4.5 Å) are indicated with red makers. At 235 K (image a) the image is divided into nine 700 × 700 pixel spatial segments, and the local lattice distortion is calculated in each segment. (c) Distribution of the number coherent HS domains of various sizes, plotted according to the number of atoms in a domain, 235 K. The black solid line in panel c is a fit to a log-normal distribution. Inset: the same data plotted on a log scale and the spatial segmentation of the TEM image for panel a. (d) Distribution of the number of coherent HS domains of various sizes at 250 K. The black solid lines in panel d fit a log-normal distribution; the insets shows the plot on a log scale along with the TEM image used for the data analysis at 250 K.

as Eshelby inclusions with shape and size different from the hosting cavity.[22] Therefore, a stress field at the interface and inside the domains (for smaller coherent structures) is expected, induced by the lattice parameter misfit between the HS and the LS states. This picture is consistent with the X-ray diffraction analysis, which showed unrelaxed lattice constants for the HS fraction.[8b,10]

The presence of a large number of irregular domains (Figure S4) suggests that there are multiple processes influencing the transition. The stoichiometry of $K_{0.3}Co[Fe(CN)_6]_{0.77}\cdot nH_2O$ dictates that there are random cyanometallate vacancies in the lattice with K^+ ions disordered in the interstices. The presence of defects has a profound impact on the mediation of the elastic interactions (the volume change). Vacancies or substitution of cyanide ligands by water molecules favors the HS Co species,[23] which provide sites of nucleation in the LS → HS transition. At the same time, the defects hinder the domain propagation by weakening the elastic interactions. These structural observations for $K_{0.3}Co[Fe(CN)_6]_{0.77}\cdot nH_2O$ are also consistent with the spin-glass like character of the IM phase, detected using bulk magnetic susceptibility measurements, that often characterizes this family of compounds.[8c,24]

CONCLUSION

The use of an ionic liquid has enabled the direct TEM observation of local atomic structure at different temperatures during a solid−solid phase transition in the coordination polymer $K_{0.3}Co[Fe(CN)_6]_{0.77}\cdot nH_2O$. The ionic liquid prevents the electron beam damage normally encountered during TEM observation of porous coordination polymers or metal−organic frameworks, and this approach should have profound impact on studies of these classes of materials.

Images evidence the elastic nature of the coordination polymer crystal and the existence of many defects. Nevertheless, the spatial distribution of the Co−Fe distances as the solid undergoes the CTIST was directly measured. At low temperature, a snapshot of the previously identified $K_{0.3}Co[Fe(CN)_6]_{0.77}\cdot nH_2O$ intermediate (IM) state reveals the existence of small coherence length HS structures randomly scattered within the LS lattice. As the temperature increases, Co−Fe distances clearly lengthen as the CTIST progresses,

DOI: 10.1021/jacs.5b08242
J. Am. Chem. Soc. 2015, 137, 14686−14693

allowing a trace of the HS domain growing and coarsening on a nanoscopic scale.

The ability to directly observe crystal elasticity was used here to quantify spatial changes in local elastic properties for a mixture of phases during a phase change, but could be extended to other analyses such as fractal shape of the HS/LS interfaces upon phase transition. Furthermore, it can be expected that direct TEM observation becomes an important analytical technique for understanding local structure during elastic transformations associated with a range of functions of coordination polymer materials, including ion storage, gas sorption, and other host−guest processes.

■ ASSOCIATED CONTENT

Supporting Information

The Supporting Information is available free of charge on the ACS Publications website at DOI: 10.1021/jacs.5b08242.

Magnetization data at 6 K, effects of electron beam dose and stability in ionic liquids, distribution of particle sizes, additional room-temperature TEM images (PDF)

■ AUTHOR INFORMATION

Corresponding Authors

*itoi.miho@nihon-u.ac.jp

*talham@chem.ufl.edu

Notes

The authors declare no competing financial interest.

■ ACKNOWLEDGMENTS

The authors thank Professor Dr. Miyashita, Professor Dr. C. Enachescu, Dr. I. Maurin, Dr. S. Otake, Dr. K. Tashiro, Dr. Y. Sato, Dr. R. Inoue, and Dr. M. Sy for helpful discussion. Two kinds of hydrophobic ILs were produced by Professor K. Tsunashima in the National Institute of Technology, Wakayama College. This work was carried out under the Visiting Researcher's Program of the Institute for Solid State Physics, the University of Tokyo. Partial support by the U.S. National Science Foundation via award DMR-1405439 (D.R.T.) is gratefully acknowledged. M.I. would like to thank UVSQ and CNRS for financial support as an invited researcher.

■ REFERENCES

(1) (a) Kitagawa, S.; Kitaura, R.; Noro, S.-i. *Angew. Chem., Int. Ed.* **2004**, *43*, 2334−2375. (b) Corma, A.; Garcia, H.; Llabrés, i.; Xamena, F. X. *Chem. Rev.* **2010**, *110*, 4606−4655. (c) Ohkoshi, S.-i.; Tokoro, H. *Acc. Chem. Res.* **2012**, *45*, 1749−1758.

(2) (a) Alamri, H.; Ballot, N.; Long, J.; Guari, Y.; Larionova, J.; Kleinke, K.; Kleinke, H.; Prouzet, E. *Chem. Mater.* **2014**, *26*, 875−885. (b) Talham, D. R.; Meisel, M. W. *Chem. Soc. Rev.* **2011**, *40*, 3356−3365. (c) Risset, O. N.; Quintero, P. A.; Brinzari, T. V.; Andrus, M. J.; Lufaso, M. W.; Meisel, M. W.; Talham, D. R. *J. Am. Chem. Soc.* **2014**, *136*, 15660−15669. (d) Presle, M.; Maurin, I.; Maroun, F.; Cortès, R.; Lu, L.; Sayed Hassan, R.; Larquet, E.; Guigner, J.; Rivière, E.; Wright, J. P.; Boillot, J.-P.; Gacoin, T. *J. Phys. Chem. C* **2014**, *118*, 13186−13195. (e) Catala, L.; Brinzei, D.; Prado, Y.; Gloter, A.; Stephan, O.; Rogez, G.; Mallah, T. *Angew. Chem., Int. Ed.* **2009**, *48*, 183−187. (f) Betard, A.; Fischer, R. A. *Chem. Rev.* **2012**, *112*, 1055−1083.

(3) (a) Imanishi, N.; Morikawa, T.; Kondo, J.; Yamane, R.; Takeda, Y.; Yamamoto, O.; Sakaebe, H.; Tabuchi, M. *J. Power Sources* **1999**, *81*−*82*, 530−534. (b) Okubo, M.; Asakura, D.; Mizuno, Y.; Kudo, T.; Zhou, H.; Okazawa, A.; Kojima, N.; Ikedo, K.; Mizokawa, T.; Honma, I. *Angew. Chem., Int. Ed.* **2011**, *50*, 6269−6273. (c) Asakura, D.; Li, C. H.; Mizuno, Y.; Okubo, M.; Zhou, H.; Talham, D. R. *J. Am. Chem. Soc.* **2013**, *135*, 2793−2799. (d) Pasta, M.; Wessells, C. D.; Liu, N.; Nelson, J.; McDowell, M. T.; Huggins, R. A.; Toney, M. F.; Cui, Y. *Nat. Commun.* **2014**, *5*, 3007. (e) Wang, L.; Lu, Y.; Liu, J.; Xu, M.; Cheng, J.; Zhang, D.; Goodenough, J. B. *Angew. Chem., Int. Ed.* **2013**, *52*, 1964−1967.

(4) (a) Chapman, K. W.; Chupas, P. J.; Kepert, C. J. *J. Am. Chem. Soc.* **2006**, *128*, 7009−7114. (b) Goodwin, A. L.; Chapman, K. W.; Kepert, C. J. *J. Am. Chem. Soc.* **2005**, *127*, 17980−17981. (c) Adak, S.; Daemen, L. L.; Nakotte, H. *J. Phys.: Conf. Ser.* **2010**, *251*, 012007.

(5) Tokoro, H.; Ohkoshi, S.-i. *Dalton Trans.* **2011**, *40*, 6825−6833.

(6) (a) Sato, O.; Iyoda, T.; Fujishima, A.; Hashimoto, K. *Science* **1996**, *272*, 704−705. (b) Sato, O.; Einaga, Y.; Iyoda, T.; Fujishima, A.; Hashimoto, K. *J. Electrochem. Soc.* **1997**, *144*, L11−L13. (c) Bleuzen, A.; Lomenech, C.; Escax, V.; Villain, F.; Varret, F.; Cartier dit Moulin, C.; Verdaguer, M. *J. Am. Chem. Soc.* **2000**, *122*, 6648−6652. (d) Maurin, I.; Chernyshov, D.; Varret, F.; Bleuzen, A.; Tokoro, H.; Hashimoto, K.; Ohkoshi, S. *Phys. Rev. B: Condens. Matter Mater. Phys.* **2009**, *79*, 064420.

(7) (a) Cartier dit Moulin, C.; Villain, F.; Bleuzen, A.; Arrio, M.; Sainctavit, P.; Lomenech, C.; Escax, V.; Baudelet, F.; Dartyge, E.; Gallet, J.; Verdaguer, M. *J. Am. Chem. Soc.* **2000**, *122*, 6653−6658. (b) Yokoyama, T.; Ohta, T.; Sato, O.; Hashimoto, K. *Phys. Rev. B: Condens. Matter Mater. Phys.* **1998**, *58*, 8257−8266. (c) Escax, V.; Champion, G.; Arrio, M.; Zacchigna, M.; Cartier dit Moulin, C.; Bleuzen, A. *Angew. Chem., Int. Ed.* **2005**, *44*, 4798−4801.

(8) (a) Park, J.-H.; Frye, F.; Anderson, N. E.; Pajerowski, D. M.; Huh, Y. D.; Talham, D. R.; Meisel, M. W. *J. Magn. Magn. Mater.* **2007**, *310*, 1458−1459. (b) Chong, C.; Itoi, M.; Boukheddaden, K.; Codjovi, E.; Rotaru, A.; Varret, F.; Frye, F. A.; Talham, D. R.; Maurin, I.; Chernyshov, D.; Castro, M. *Phys. Rev. B: Condens. Matter Mater. Phys.* **2011**, *84*, 144102. (c) Pajerowski, D. M.; Garlea, V. O.; Knowles, E. S.; Andrus, M. J.; Dumont, M. F.; Calm, Y. M.; Nagler, S. E.; Tong, X.; Talham, D. R.; Meisel, M. W. *Phys. Rev. B: Condens. Matter Mater. Phys.* **2012**, *86*, 054431.

(9) Itoi, M.; Maurin, I.; Varret, F.; Frye, F. A.; Talham, D. R.; Chernyshov, D.; Boukheddaden, K. *Phys. Rev. B: Condens. Matter Mater. Phys.* **2013**, *88*, 094104.

(10) Andrus, M. J.; Calm, Y. M.; Knowles, E. S.; Dumont, M. F.; Abboud, K. A.; Meisel, M. W.; Talham, D. R. *Polyhedron* **2013**, *64*, 289−293.

(11) (a) Rasband, W. S. *ImageJ*; U. S. National Institutes of Health: Bethesda, MD, 1997−2014; http://imagej.nih.gov/ij/. (b) Schneider, C. A.; Rasband, W. S.; Eliceiri, K. W. *Nat. Methods* **2012**, *9*, 671−675. (c) Abramoff, M. D.; Magalhaes, P. J.; Ram, S. J. *Biophotonics Int.* **2004**, *11* (7), 36−42.

(12) (a) Hytch, M. J. *Scanning Microsc.* **1997**, *11*, 53−66. (b) Diercks, D.; Lian, G.; Chung, J.; Kaufman, M. *J. Microsc.* **2011**, *241* (pt2), 195−199. (c) Hÿtch, M. J.; Snoeck, E.; Kilaas, R. *Ultramicroscopy* **1998**, *74*, 131−146. (d) Kundu, P.; Turner, S.; Van Aert, S.; Ravishankar, N.; Van Tendeloo, G. *ACS Nano* **2014**, *8*, 599−606.

(13) Egerton, R. F.; Li, P.; Malac, M. *Micron* **2004**, *35*, 399−409.

(14) Torimoto, T.; Tsuda, T.; Okazaki, K.; Kuwabata, S. *Adv. Mater.* **2010**, *22*, 1196−1221.

(15) (a) Kuwabata, S.; Kongkanand, A.; Oyamatsu, D.; Torimoto, T. *Chem. Lett.* **2006**, *35*, 600−601. (b) Arimoto, S.; Oyamatsu, D.; Torimoto, T.; Kuwabata, S. *ChemPhysChem* **2008**, *9*, 763−767. (c) Tsuda, T.; Mochizuki, E.; Kishida, S.; Nemoto, N.; Ishigaki, Y.; Kuwabata, S. In *Molten Salts Chemistry and Technology*; Gaune-Escard, M., Haarberg, G., Eds.; John Wiley & Sons: Chichester, U.K., 2014; pp 373−389.

(16) Uematsu, T.; Baba, M.; Oshima, Y.; Tsuda, T.; Torimoto, T.; Kuwabata, S. *J. Am. Chem. Soc.* **2014**, *136*, 13789−13797.

(17) Miyashita, S.; Konishi, Y.; Nishino, M.; Tokoro, H.; Rikvold, P. A. *Phys. Rev. B: Condens. Matter Mater. Phys.* **2008**, *77*, 014105.

(18) Slimani, A.; Boukheddaden, K.; Varret, F.; Oubouchou, H.; Nishino, M.; Miyashita, S. *Phys. Rev. B: Condens. Matter Mater. Phys.* **2013**, *87*, 01411.

(19) (a) Katsuragi, H.; Sugino, D.; Honjo, H. *Phys. Rev. E* **2004**, *70*, 065103. (b) Kadono, T.; Arakawa, M. *Phys. Rev. E: Stat. Phys., Plasmas, Fluids, Relat. Interdiscip. Top.* **2002**, *65*, 035107.

(20) (a) Slimani, A.; Varret, F.; Boukheddaden, K.; Garrot, D.; Oubouchou, H.; Kaizaki, S. *Phys. Rev. Lett.* **2013**, *110*, 087208. (b) Sy, M.; Varret, F.; Boukheddaden, K.; Bouchez, G.; Marrot, J.; Kawata, S.; Kaizaki, S. *Angew. Chem., Int. Ed.* **2014**, *53*, 7539−7542. (c) Nishino, M.; Boukheddaden, K.; Konishi, Y.; Miyashita, S. *Phys. Rev. Lett.* **2007**, *98*, 247203. (d) Enachescu, C.; Nishino, M.; Miyashita, S.; Hauser, A.; Stancu, A.; Stoleriu, L. *Europhys. Lett.* **2010**, *91*, 27003.

(21) Chong, C.; Mishra, H.; Boukheddaden, K.; Denise, S.; Bouchez, G.; Collet, E.; Ameline, J.; Naik, A. D.; Garcia, Y.; Varret, F. *J. Phys. Chem. B* **2010**, *114*, 1975−1984.

(22) (a) Seitz, D.; Turnbull, D. *Solid State Physics: Advances in Research and Applications*; Academic Press: New York, 1956; Vol. 3. (b) Willenbacher, N.; Spiering, H. *J. Phys. C: Solid State Phys.* **1988**, *21*, 1423. (c) Spiering, H.; Willenbacher, N. *J. Phys.: Condens. Matter* **1989**, *1*, 10089. (d) Boukheddaden, K. *Phys. Rev. B: Condens. Matter Mater. Phys.* **2013**, *88*, 134105. (e) Eshelby, J. D. *Philos. Trans. R. Soc., A* **1951**, *244*, 87.

(23) Kawamoto, T.; Asai, Y.; Abe, S. *Phys. Rev. B: Condens. Matter Mater. Phys.* **1999**, *60*, 12990−12993.

(24) Pejaković, D. A.; Manson, J. L.; Miller, J. S.; Epstein, A. J. *Phys. Rev. Lett.* **2000**, *85*, 1994−1997.

DOI: 10.1021/jacs.5b08242
J. Am. Chem. Soc. 2015, 137, 14686−14693